

Confinement of Toroidal Non-neutral Plasma in Proto-RT

Haruhiko Saitoh*, Zensho Yoshida* and Sho Watanabe*

**Graduate School of Frontier Sciences, University of Tokyo,
5-1-5 Kashiwanoha, Kashiwa, Chiba 277-8583, Japan*

Abstract. In contrast to linear configurations for non-neutral plasmas, toroidal devices allow us to trap charged particles without the use of a plugging electric field. Thus it has a potential ability to confine high-energy particles or to simultaneously trap multiple particles with different charges. In spite of the relatively long history of the study in pure toroidal magnetic field devices, toroidal non-neutral plasmas are attracting renewed interest with the use of magnetic surface configurations [1, 2]. Possible applications of toroidal trap for non-neutral plasmas are formation of matter-antimatter plasmas [2], investigation on the fundamental properties of exotic plasmas including pair (equal mass) plasmas, and experimental test on the equilibrium and stability of flowing plasmas [3, 4, 5]. As an initial test on non-neutral plasmas in the toroidal magnetic-surface geometry, formation and confinement properties of pure electron plasma have been investigated at Prototype-Ring Trap (Proto-RT) device with a dipole magnetic field [1, 6, 7]. Electrons can be injected by using chaotic orbit near a magnetic null line generated by the combination of dipole and vertical magnetic fields [6]. The confinement time of electrons is limited due to the effects of collisions with remaining neutral gas, and electrons of $\sim 10^{12}$ are trapped for ~ 0.5 s in the typical magnetic field strength of 100 G and back pressure of 4×10^{-7} Torr in Proto-RT. Although the present experiment was carried out on the single-component plasma, the result shows that a stable confinement configuration has been realized for toroidal non-neutral plasmas by using the magnetic surface configuration. Together with the experiment on the toroidal pure electron plasma in Proto-RT, preliminary prospects for the injection and trap of anti-protons and positrons in the toroidal magnetic surface configuration, and creation of multi-component plasmas will be described.

Keywords: Non-neutral plasma, electron plasma, toroidal geometry, magnetic surface configuration, antimatter plasmas

PACS: 52.27.Jt, 52.27.Aj, 52.35.Fp

I. INTRODUCTION

Confinement of non-neutral plasmas in a toroidal geometry

In recent years, it has been recognized that toroidal geometries might be suitable for the various kinds of non-neutral plasmas [1, 2]. Although excellent confinement properties of single-component plasmas are realized in Malmberg-Penning traps [8], and also the partial overlap of negatively and positively charged particles is successfully demonstrated in a “nested” Penning trap [9, 10], it is not straightforward to simultaneously confine both charges with satisfying

$$\lambda_D \ll L, \tag{1}$$

which is an essential criteria for the observation of plasma phenomena. Here λ_D is the Debye length of each component of particles defined as $\lambda_D \equiv (\epsilon_0 T / ne^2)^{1/2}$, where ϵ_0 is

the dielectric constant of vacuum, T is the temperature, n is the number density, e is the charge of particles, and L is the scale size of the plasma. In contrast to linear traps for non-neutral plasmas, toroidal devices can produce closed magnetic field lines inside the device geometry. Thus it has a potential ability to confine charged particles at any degree of non-neutrality, or to trap high-energy beam particles and multiple species of different charges, without the use of plugging electric field. Mirror, cusp, and hybrid Penning-Paul devices can also trap multi-component plasmas, and the toroidal geometry is one of the candidates for the simultaneous confinement of both species of particles.

The realization of the stable confinement of multi-component non-neutral plasma will make possible various experiments in the fields of atomic and plasma physics. One of the possible applications of multi-component plasma traps is the formation of matter-antimatter plasmas [1, 2]. These experiments include the creation of antiproton or positron plasmas and their mixtures, such as antihydrogen plasmas. Because the “overlap” scale length of both species are not limited to $\sim \lambda_D$ caused by the electrostatic forces, the pure magnetic field confinement in the toroidal geometry is potentially useful for the efficient creation of antihydrogen atoms. A positron-electron plasma is a so-called pair plasma with equal-mass particles, and several unique properties on wave propagations are theoretically predicted. A positron-electron plasma is also expected to play important roles in many astrophysical phenomena, although little is known about the experimental issue in laboratory plasmas.

As well as the investigation on the properties of such kinds of exotic plasmas, fundamental experimental test on the equilibrium and stability of a flowing plasma (double Beltrami state) [3, 4, 5] is also possible in a toroidal geometry. When the velocity of plasma flow is comparable to the Alfvén speed, the plasma pressure can be balanced by the dynamic pressure of the flow, and it will open a new path toward the advanced fusion concept. The required flow can be induced by the drift motion of a non-neutralized plasma in the toroidal geometry. Thus the creation of a toroidal multi-component non-neutral plasma will form a basis for many scientific applications.

Pure toroidal magnetic field configuration

Studies on toroidal non-neutral plasmas have been carried out in a pure toroidal magnetic field [11, 12, 13, 14, 15, 16, 17, 18, 19, 20, 21]. An interesting equilibrium state was revealed in these experiments, one is in marked contrast to the confinement of a neutral plasma, which requires rotational transforms of magnetic field lines in order to avoid the drift loss of particles. In the drift orbit approximation, the total energy of a charged particle in a toroidal magnetic field is

$$E = q\phi + \frac{\mu_0 B_0 R_0}{R} + \frac{L_z^2}{2mR} + \frac{m(\nabla\phi)^2}{2B^2}, \quad (2)$$

where q is charge, ϕ is the electrostatic potential, R_0 is the major radius, B_0 is the magnetic field strength at $R = R_0$, μ_0 is the space permeability, L_z is the angular momentum of the particle around z axis, and m is the particle mass. Because the total energy of each particle is conserved, surfaces defined by $E = \text{const.}$ constrain the positions of the

guiding center of the particles. When there is no electric field (neutral plasmas), Eq. (2) becomes

$$E = \frac{\mu_0 B_0 R_0}{R} + \frac{L_z^2}{2mR} \propto 1/R, \quad (3)$$

and the guiding center motions are on cylinders, which inevitably intersects the boundary wall of a containing chamber. In non-neutral plasmas, however, due to the strong radial electric field caused by the space and image charges, $E = \text{const.}$ surfaces can take closed circular shape in the poloidal cross section of the torus. The particles might also take closed orbits in a pure toroidal field undergoing the poloidal $\mathbf{E} \times \mathbf{B}$ rotation [12] according to the trap configuration. In a conducting toroidal vessel, the particles can take closed orbits due to the $\mathbf{E} \times \mathbf{B}$ rotation, which is inward-shifted from the equipotential contours because of the other first order drifts. By substituting $\mathbf{E} \times \mathbf{B}$ drift speed $\mathbf{v} = -\nabla\phi \times \mathbf{B}/B^2$, the steady state continuity equation $\nabla \cdot (n\mathbf{v}) = 0$ becomes

$$\left[\nabla\phi \times \nabla \left(\frac{n}{B^2} \right) \right] \cdot \mathbf{B} = 0. \quad (4)$$

When electric and magnetic fields and plasmas are axisymmetric, Eq. (4) implies that

$$\frac{n}{B^2} = f(\phi). \quad (5)$$

By using Eq. (5), one can solve Poisson's equation

$$\nabla^2 \phi = -\frac{nq}{\epsilon_0} \quad (6)$$

in order to obtain equilibrium potential and density profiles of toroidal non-neutral plasmas.

The early experiments of toroidal electron plasmas were conducted for the storage or acceleration of heavy ions [13] or creation of high-current relativistic electron beams [15]. In a series of experiments in low-aspect-ratio torus devices [18, 19], toroidal effects, electron injection methods, and other collective behaviors of electron plasma were studied. Existence of the above mentioned equilibrium of electron plasma in pure toroidal field was demonstrated in these experiments. An electrostatic force balance equilibrium model, including the effects of the space and image charges, was also studied [17]. Toroidal electron plasmas feel repulsive ‘‘hoop force’’ caused by the self electric field and also by the diamagnetic effects, and the confinement can be achieved by the external radial electric fields due to the image charges on the vessel wall or electrodes.

Toroidal magnetic surface configuration

Magnetic surface configurations are most efficient trap devices for plasmas and are intensively studied in the field of high temperature fusion plasma research. In a simple torus device with a pure toroidal magnetic field B_ϕ , the inhomogeneous field strength ($\propto 1/R$) induces the vertical charge separation, which lead to the outward $\mathbf{E} \times \mathbf{B}$ loss

of the both particles. In order to avoid such rapid loss of plasmas, a poloidal field plays essential role in order to form closed magnetic surfaces. Poloidal fields are generated by means of an internal plasma current (tokamaks), an external coil current (stellarators), or an internal coil current (internal conductor and multi-pole devices).

Magnetic surfaces are defined as $\psi(\mathbf{r}) = \text{const.}$ planes, where magnetic field lines lie on $\psi(\mathbf{r}) = \text{const.}$ and thus

$$\nabla\psi(\mathbf{r}) \cdot \mathbf{B} = 0 \quad (7)$$

is satisfied. When the magnetic field configuration is axisymmetric, the analytic representation of the magnetic surfaces is

$$\psi = rA_\theta(r, z) = \text{const.} \quad (8)$$

and a poloidal field is given by

$$B_r = -\frac{1}{r} \frac{\partial\psi}{\partial z} \quad \text{and} \quad B_z = \frac{1}{r} \frac{\partial\psi}{\partial r}, \quad (9)$$

which satisfies Eq. (7).

The Lagrangian equation of the motion of a charged particle in a magnetic field \mathbf{B} and an electric field \mathbf{E} is given by

$$\frac{d}{dt} \left(\frac{\partial L}{\partial \dot{q}_i} \right) - \frac{\partial L}{\partial q_i} = 0, \quad (10)$$

where

$$L = \frac{mv^2}{2} + q\mathbf{v} \cdot \mathbf{A} - q\phi. \quad (11)$$

Here \mathbf{A} is the vector potential: $\mathbf{B} = \nabla \times \mathbf{A}$ and ϕ is the scalar potential: $\mathbf{E} = -\nabla\phi$, and \mathbf{q} is the coordinate of the charged particle. In a toroidally symmetric configuration ($\partial/\partial\theta = 0$), the canonical angular momentum of the charged particle satisfies

$$P_\theta \equiv \frac{\partial L}{\partial \dot{\theta}} = mr^2\dot{\theta} + qrA_\theta = \text{const.} \quad (12)$$

The variation of ψ at a distance d from ψ at the initial point is given by

$$|\delta\psi| = d|\nabla\psi|, \quad (13)$$

and by using Eq. (12), d is calculated as

$$d = \left| \frac{m\delta(rv_\theta)}{q|\nabla\psi|} \right|. \quad (14)$$

From Eqs. (8) and (9), $|\nabla\psi| = r(B_r^2 + B_z^2)^{1/2} = rB_p$ and also assuming that $\delta(rv_\theta) < \sim rv_\theta$, the maximum value of d is given by

$$d \leq \left| \frac{mr\dot{\theta}}{qB_p} \right| \equiv r_{Lp}, \quad (15)$$

indicating that the deviation of the charged particle from one magnetic surface is less than the poloidal Larmor radius r_{Lp} . When the magnetic field is strong enough and the mechanical momentum of a particle is ignored, the canonical angular momentum of the particle is approximated as

$$P_\theta \sim qrA_\theta, \quad (16)$$

and the orbits of charged particles are limited on magnetic surfaces.

When the Hamiltonian of the charged particle

$$H = -L + \sum_i p_i \dot{q}_i = -\frac{1}{2m}(\mathbf{p} - q\mathbf{A})^2 + q\phi \quad (17)$$

is not explicitly time dependent, the total energy of the charged particles is conserved:

$$W = \frac{mv^2}{2} + q\phi = \text{const}. \quad (18)$$

and v has an upper limit of $v \leq (2(W - q\phi)/m)^{1/2}$, and thus, as long as the poloidal field lines form closed magnetic surfaces in a finite region, the orbits of charged particles are also limited to a finite region.

The force balance equation of single component non-neutral plasma is

$$mn \left(\frac{\partial \mathbf{v}}{\partial t} + \mathbf{v} \cdot \nabla \mathbf{v} \right) = qn(\mathbf{v} \times \mathbf{B} - \nabla \phi) - \nabla p. \quad (19)$$

When the density of non-neutral plasmas is far below the Brillouin limit

$$n_B = \frac{\epsilon_0 B^2}{2m}, \quad (20)$$

and the pressure term is negligibly smaller than the electromagnetic forces, the equation of motion reduces to

$$qn(\mathbf{v} \times \mathbf{B} - \nabla \phi) = 0. \quad (21)$$

By taking the scalar product of Eq. (21) and \mathbf{B} ,

$$\mathbf{B} \cdot \nabla \phi = 0, \quad (22)$$

indicating that the electrostatic potential is constant on a magnetic field line. From Eq. (21), the perpendicular velocity of the fluid is given by the $\mathbf{E} \times \mathbf{B}$ drift speed

$$\mathbf{v} = -\frac{\nabla \phi \times \mathbf{B}}{B^2}, \quad (23)$$

and the strong self electric field of non-neutral plasmas induces fast cross-field transport of charged particles on a magnetic surface. Thus in cold non-neutral plasmas, electrostatic potential ϕ is a function of magnetic flux ψ

$$\phi = \phi(\psi). \quad (24)$$

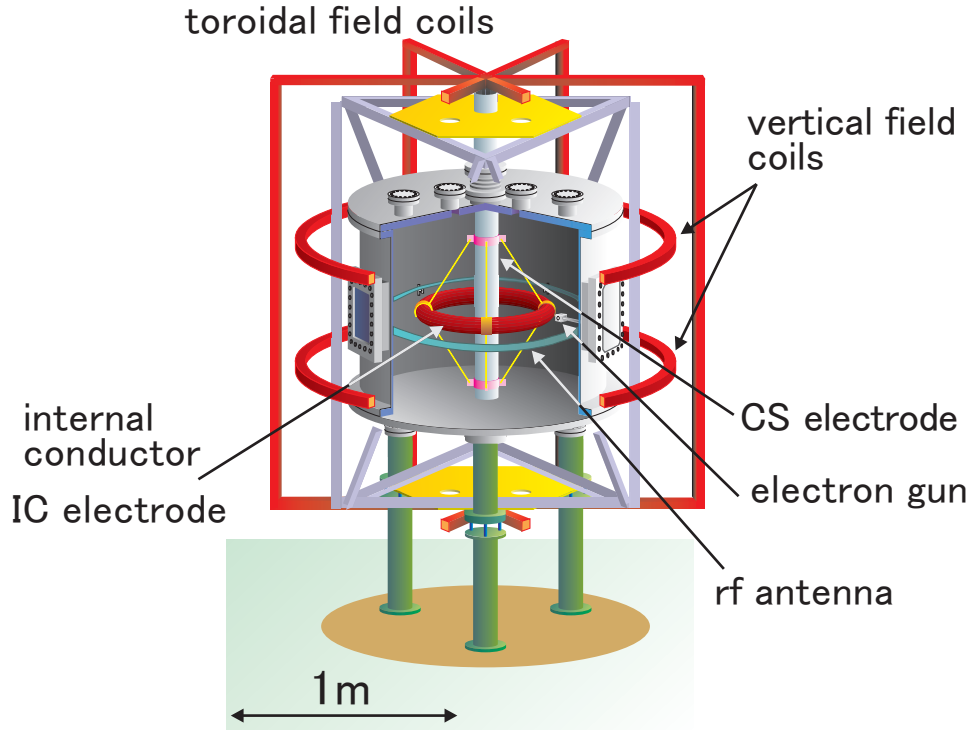


FIGURE 1. Bird eye view of the Proto-RT device.

When the temperature of the plasma is also a function of magnetic flux ψ , the density in the equilibrium state is given by

$$n = N(\psi) \exp \frac{e\phi}{k_B T_e(\psi)}, \quad (25)$$

and one may solve Poisson's equation

$$\nabla^2 \phi = \frac{1}{\epsilon_0} N(\psi) \exp \frac{e\phi}{k_B T_e(\psi)} \quad (26)$$

to obtain equilibrium potential and density profiles of toroidal electron plasmas[2].

Magnetic surface devices for non-neutral plasmas

Until very recently, little attention has been given to the confinement of non-neutral plasmas on magnetic surfaces. As well as the improvement of the confinement properties of toroidal non-neutral plasmas, the use of magnetic surface configuration is essentially important for the trap of multi-component plasmas (e.g. antihydrogen plasma or positron-electron plasma) in a toroidal geometry, in order to avoid the above mentioned charge separation and the resultant rapid loss of particles.

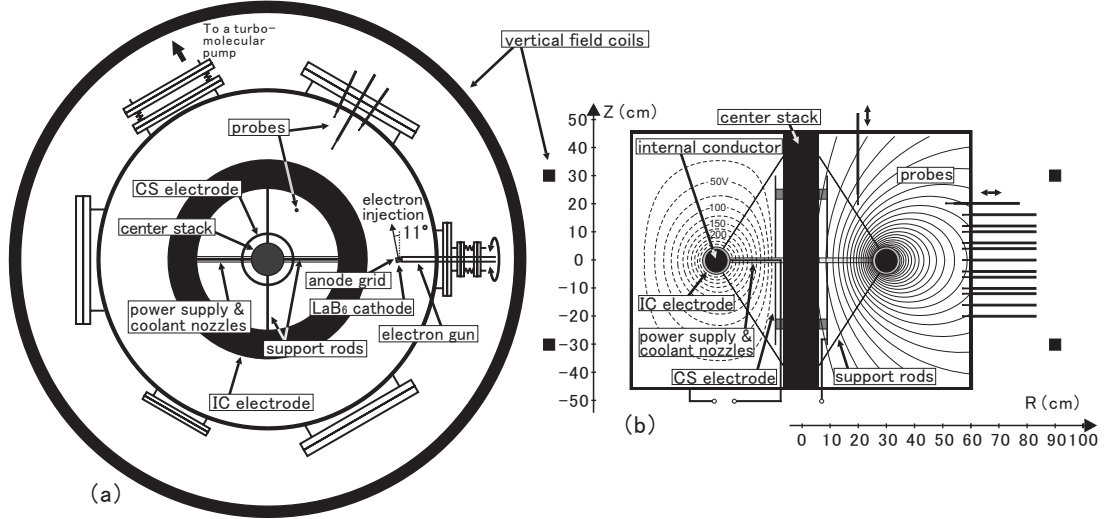


FIGURE 2. (a) Top view and (b) poloidal cross section of Proto-RT. Magnetic surfaces of a dipole field and equi-potential contours when the IC electrode is biased are also shown.

For the confinement of low density (below the Brillouin limit n_B) non-neutral plasmas, current-free configurations are suitable for the generation of magnetic surfaces. Closed magnetic surfaces of a dipole field can be produced by a ring conductor hung in a vacuum vessel. For the reduction of disturbance due to the mechanical structures of the coil support, one may use a super-conducting levitated coil ring [1]. As a first step toward the realization of an antiproton plasma, a positron plasma, and other multi-component plasmas with a radial electric field in a toroidal geometry, a pure electron plasma is relatively easy to generate, and is suitable for the fundamental test on the various toroidal non-neutral plasmas.

Proto-RT is a prototype ring trap device constructed for the investigation of various topics in non-neutral plasma physics, and experiments on a toroidal pure electron plasma has been carried out. In the following sections, recent experimental investigation in Proto-RT, including the plasma formation, confinement properties, and electrostatic potential structures of a toroidal electron plasma are described.

II. EXPERIMENTAL SETUP IN PROTO-RT

Device and magnetic field configuration

The Proto-RT device is an internal conductor device constructed in 1998 for the study of physics related to non-neutral plasmas [1], chaos-induced resistivity of collisionless plasma and its application to low-gas-pressure plasma sources [22, 23], and experimental investigation of ultra-high β plasma with fast flow [3, 4]. The bird-eye view and cross sections of Proto-RT are described in Figs. 1 and 2.

Proto-RT consists of a cylindrical chamber, three kinds of magnetic field coils, vacuum pumps, and other diagnostic apparatus connected to the main chamber, as shown in

the figures. The chamber has a rectangular poloidal cross section of $90 \text{ cm} \times 53.3 \text{ cm}$ and it is evacuated to the base pressure of 4×10^{-7} Torr by a turbomolecular pump. Proto-RT has three kinds of magnetic field coils: internal conductor (IC), vertical field (VF) coils, and toroidal field (TF) coils, and a variety of field configurations can be produced by the combination of these coils. Inside the chamber, a ring-shaped internal conductor for the production of dipole magnetic field is hung by support rods that are connected to the center stack (CS) of 11.4 cm diameter. The major radius and minor radius of the IC case is 30 cm and 4.3 cm, respectively. Electric current and coolant for the IC are fed through a pair of tube structures via the CS. All these structures, including the support rods and coolant or feeder tubes, are covered by ceramic tubes for the electric insulation from plasmas. Outside the chamber, a pair of the vertical field coils are installed at $R = 90 \text{ cm}$ with a vertical interval of 60 cm. It provides almost parallel magnetic field lines inside the chamber, and used for deforming the shape of magnetic surfaces. For the production of magnetic shear, toroidal field coils are installed in the CS. All the coils are power fed by DC power sources and the maximum coil currents are 10.5 kAT (IC), 5.25 kAT (VF), and 30 kAT (TF), respectively. The typical strength of the magnetic field in the confinement region of the chamber is of the order of 10^{-2} T. Magnetic surfaces in the poloidal cross section of the Proto-RT chamber are shown in Fig. 2 as solid lines.

A toroidal non-neutral plasma relaxes to an equilibrium state under the effects of external electric fields from outside of the space charges [17]. As far as an equilibrium state is found, this external fields are automatically generated by the induced image charges on the chamber. The equilibrium can also be externally controlled by the applied electric fields generated by the electrodes. The electrodes are also effective for the potential optimization and formation of radial electric field inside neutral plasmas. In this study, the effects of electrode biasing were examined. For the potential optimization and formation of radial electric field inside the plasma, a pair of electrode are installed on the IC and the CS. The dotted lines in Fig. 2 show the equi-potential contours when the IC electrode is biased to $V_{IC} = 300 \text{ V}$.

Electron injection

An electron gun is installed in Proto-RT at the peripheral location of the confinement region as shown in Fig. 3. A lanthanum hexaboride (LaB_6 , work function is $\phi_W = 2.6 \text{ eV}$) sintered compact is employed as a cathode of the electron gun. The electron gun is located near $Z = 0$ plane, and it is movable in the radial direction. Injection angle of the gun is also variable using a rotating flange. Acceleration voltage of up to $V_{acc} = 1.3 \text{ kV}$ is applied between the LaB_6 cathode and a molybdenum anode grid of 65 % transparency, located 2 mm in front of the cathode. The cathode is heated with a current of up to 28 A by a regulated DC power source and operated at temperature of $\sim 1800 \text{ K}$. Acceleration voltage V_{acc} is controlled by a MOS-FET open-drain semiconductor switch. The obtained drain current is $I_{drain} \sim 0.8 \text{ A}$ when $V_{acc} = 1.2 \text{ kV}$ and no magnetic field. With $V_{acc} = 300 \text{ V}$, the electron injection beam current I_{beam} is 26 mA when V_{IC} (IC electrode bias voltage) is 0, and 5.9 mA when $V_{IC} = -300 \text{ V}$. The gun

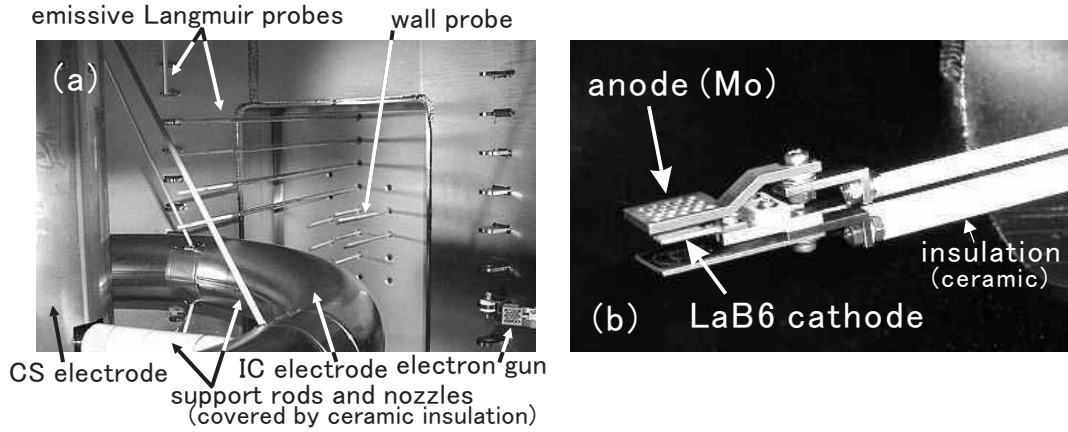


FIGURE 3. (a) Internal view of Proto-RT and (b) electron gun structure.

is usually operated at a base pressure of below 1×10^{-5} Torr, in order to avoid rapid evaporation and evaporation coating due to the oxidation of the cathode.

The injection angle of the electron gun is decided according to a numerical calculation [6] so that the electrons take sufficiently long orbit lengths. Because of the large gyration radius, electrons obey a strongly nonlinear equation of motion in the inhomogeneous magnetic field, resulting in chaotic (non-periodic) motion with long orbit lengths. A numerical calculation shows that electrons are effectively injected from the edge of the confinement region [6]. The typical orbit of a single electron injected into a dipole magnetic field is shown in Fig. 4 (bird-eye view where $X = Y = 0$ is the center axis of the device). When the pitch angle between the dipole magnetic field lines and initial injection velocity is large, electrons take transit orbit around the IC as shown in Fig. 4 (a). Electrons with small parallel velocities are mirror trapped in the bad curvature region (Fig. 4 (b)). Electrons also undergo the Larmor rotation around the magnetic field lines, and drift motion in the toroidal direction due to the $\mathbf{E} \times \mathbf{B}$ and $\nabla B/\text{curvature}$ drifts.

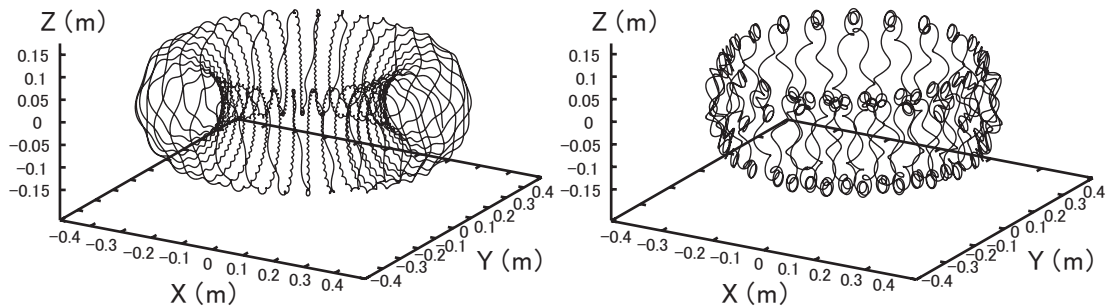


FIGURE 4. Typical electron trajectories of (a) “passing” and (b) “trapped” orbits.

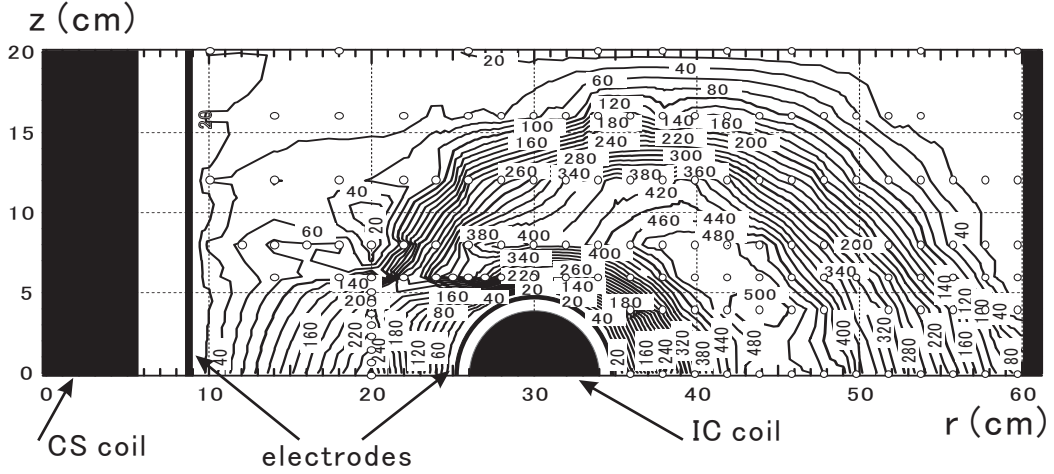


FIGURE 5. Measuring points of Langmuir probes and an example of the reconstructed potential profile.

Diagnostics on toroidal electron plasma

Among other parameters, space potential ϕ_s is one of the essential parameters for the measurements of the structures of pure electron plasmas. The electrostatic potential of the plasma is measured by emissive Langmuir probes and it provides the information of potential profiles with fine spatial resolution. Basically, the probe is a simple metallic tip inserted into a plasma, and biased to some potential. Analysis of the relation between the bias voltage and the obtained current provides the information of electron parameters. For pure electron plasmas, structures like Langmuir probes inside the plasma are serious obstacles for the realization of stable confinement, but it can be used for the measurements of space potential during the electron injection phase.

The probes are arranged as an array located between $Z = -20$ cm and $+20$ cm (the configuration of the probes is shown in Fig. 2) and two dimensional potential structures are measured in the confinement region. Schematic and photographic views of emissive Langmuir probe configuration are shown in Figs. 3. The probes were inserted from gauge ports (*r-probes*) on the diagnostic flange and one gauge port (*z-probe*) on a diagnostic port. The probes are manually movable along \mathbf{r} (*r-probe*) or \mathbf{z} (*z-probe*) direction, and we can obtain two-dimensional potential profiles. Measuring points and reconstructed 2-d profiles are shown in Fig. 5.

After the stop of the electron supply, Langmuir probes placed inside the confinement region are serious obstacles for the realization of stable equilibrium. For the measurement of electrostatic fluctuations and determination of the confinement time of the plasma without such perturbations, 5×15 mm and 5×250 mm copper foils are covered by insulating quartz tubes and installed in the chamber, and used as wall probes [14]. The sensor foil is connected to the vessel wall through a current amplifier for the observation of image current, which indicates the motion of the plasma. The longer wall is placed over the entire confinement region and used for the estimation of the remaining charge of the plasma by integrating the passing image current.

Electrostatic fluctuations of the plasmas are measured by wall probes. During the

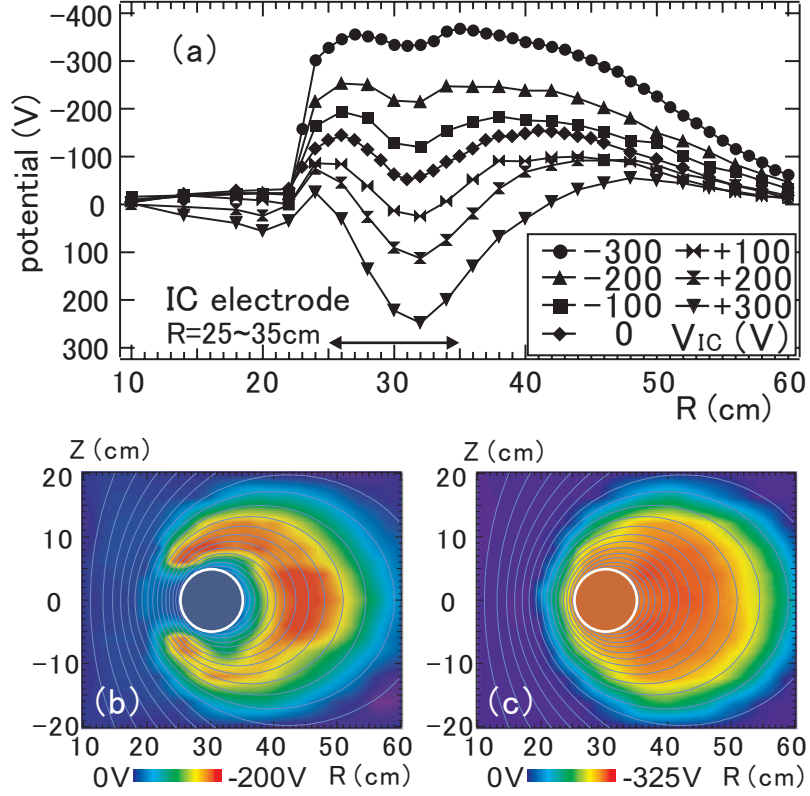


FIGURE 6. (a) Radial potential profiles of electron plasma at $Z = 6$ cm in the variation of the electrode bias voltage V_{IC} . Two dimensional potential distribution (b) when $V_{IC} = 0$ V and (c) when $V_{IC} = -300$ V. Thin lines show the magnetic surfaces of the dipole field.

electron injection, a current collected by the high-impedance emissive Langmuir probe is less than $10 \mu\text{A}$. It is much smaller than the injected beam current of the electron gun of $2 \sim 30$ mA, and the resultant disturbance is supposed to be small. In fact, additional insertion of another Langmuir probe does not significantly change the measured Φ_H , and we therefore conclude that during the electron injection, the Langmuir probes do not seriously perturb the plasma.

III. TOROIDAL ELECTRON PLASMA IN PROTO-RT

Electron injection and potential formation

Figure 6 shows the structures of the internal electric potential in the poloidal cross section of the device during the electron injection (the injection period was $100 \mu\text{s}$). Potential profiles when the IC electrode is grounded is shown in Fig. 6 (b). Poisson equation was solved in the geometry of Proto-RT [7], and we may reproduce the measured potential profile, assuming an electron cloud with a peak number density of $1 \times 10^{13} \text{ m}^{-3}$ and a total space charge of $3 \times 10^{-7} \text{ C}$. When $V_{IC} = -300$ V, the peak density and total charge are estimated to be $1 \times 10^{13} \text{ m}^{-3}$ and $4 \times 10^{-7} \text{ C}$, respectively. The high density

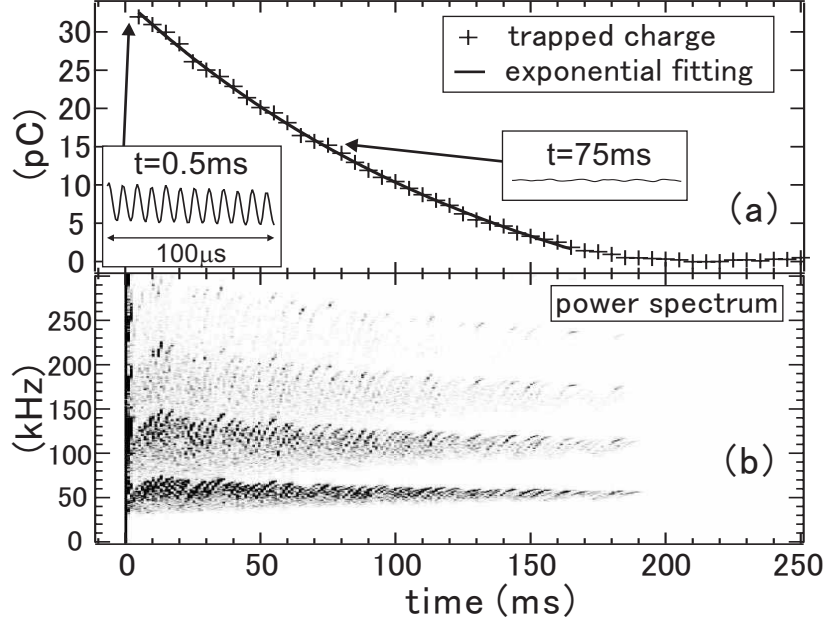


FIGURE 7. (a) Trapped charge of electron plasma after the stop of electron supply at $t = 0$ and (b) temporal evolution of the power spectrum of the electrostatic fluctuation.

region of the electron plasma is relatively remote from the support rods of the internal conductor throughout the experiments, and these structure does not seriously perturb the electron plasmas so long as the electrons rotates in the toroidal direction.

When the potential is not externally controlled (the IC electrode is grounded) in Fig 6 (b), the distribution has a reversed “C” shape and the potential contours show strong disagreement with the magnetic surfaces of the dipole field configuration. Thus the potential contours without electrode bias do not coincide with the magnetic surfaces, implying a rapid particle loss across the field lines. Because the electrostatic potential ϕ is not constant on a magnetic surface, Eq. (22) is not satisfied, implying that thermalized (low energy) electrons are not confined when the potential is not externally controlled. The injected electron beam current when $V_{IC} = 0$ V is $I_{\text{beam}} = 26$ mA, and it is an order of magnitude larger than when $V_{IC} = -300$ V, also may suggesting that stable confinement is not realized unless the IC electrode is negatively biased.

In contrast, when the IC electrode is negatively biased, the potential profile was successfully modified. Figure 6 (c) shows the potential profile when $V_{IC} = -300$ V, the same potential as the acceleration voltage of the electron gun. The potential well near the IC electrode is eliminated, and the potential contours surround the IC, which is topologically close to the shape of the magnetic surfaces.

Figure 6 (a) shows the radial potential profiles at $Z = +6$ cm, just above the surface of the IC electrode. The grounded or positively biased IC electrode yields a hollow potential profiles around the IC. These concave potential distributions are not favorable for the stable confinement, because the resultant sheared $\mathbf{E} \times \mathbf{B}$ flow can be a energy source for the destabilization of the Kelvin-Helmholtz (diocotron) modes. By negatively biasing the IC electrode, the hollow structures are cancelled as illustrated in the figure, and it

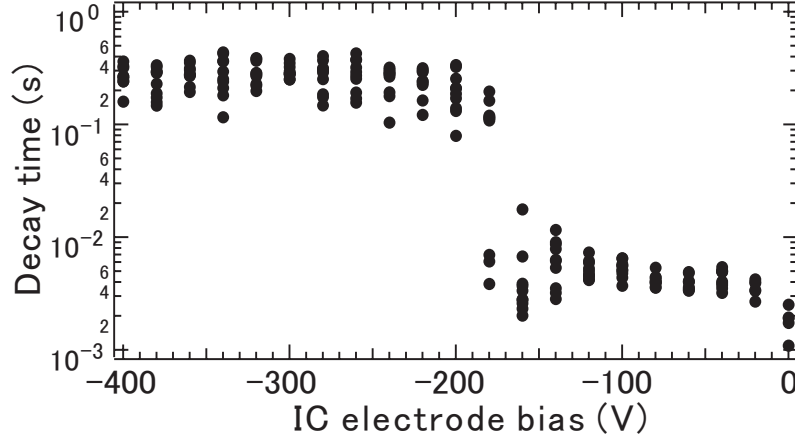


FIGURE 8. Confinement time of an electron plasma in the variation of V_{IC} .

might lead to stabilize the diocotron instability of non-neutral plasmas. As described in the next subsection, the measurements of electrostatic fluctuation show that the confinement time is enhanced for more than an order of magnitude by the negative bias of the IC electrode.

Fluctuation and trapped charge decay

The typical temporal evolution of the electron plasma, the trapped charge and the power spectrum of the electrostatic fluctuation are shown in Fig. 7. Electrons are injected with an acceleration voltage of 300 V from $t = -100$ to $0 \mu\text{s}$, into DC magnetic and electric fields generated by a dipole field coil current of $I_{IC} = 7 \text{ kAT}$ (magnetic field strength at $R = 40 \text{ cm}$ is 70 G) and electrode bias voltages of $V_{IC} = -300 \text{ V}$ and $V_{CS} = 0 \text{ V}$. After the electron gun is turned off at $t = 0 \text{ s}$, a large oscillation during the electron injection phase decays typically in a time constant of $\sim 1 \text{ ms}$. Subsequently, a quiet oscillation mode is realized only when the IC electrode is negatively biased.

The wall signals before and after the stabilization of the initial large fluctuation are shown in the small boxes in Fig. 7 (a). The magnitude of the electrostatic fluctuation before and during the quiet mode normalized by the DC electrostatic potential in the plasma is $\tilde{\phi}/\phi = 12 \%$ and 0.6% , respectively. In the quiet confinement phase, the remaining charge drops approximately exponentially as indicated in Fig. 7 (a). As the plasma enters the quiet confinement mode, the frequency of oscillation, illustrated in Fig. 7 (b), decreased from 240 kHz to 62 kHz. In the quiet confinement phase, the decrease of the frequency is relatively small, and the peak of the fundamental frequencies in the power spectrum are 62 kHz at $t = 5 \text{ ms}$ and 57 kHz at $t = 180 \text{ ms}$, indicating that both self and external electric fields decide the frequencies of the electrostatic oscillation.

The frequencies of the observed electrostatic oscillation is inversely proportional to the magnetic field strength and it shows approximately linear dependence on the external electric fields. As well as the characteristics of the fluctuation frequencies, the direction

of the wave propagation also agrees with the properties of diocotron oscillation mode.

The confinement time of the particles (time constants of the exponential fitting curves) as a function of V_{IC} is shown in Fig. 8. When V_{IC} is above -180 V, the initial fluctuation of the plasma does not enter a quiet state and the charge decays within some milliseconds. The amplitude of the initial fluctuation when $V_{IC} = -80$ V is $\tilde{\phi}/\phi = 32$ % and it decays without entering the quiet confinement mode. As indicated in Fig. 6, the drastic improvement of the confinement is observed when the hollow potential structure is eliminated by the sufficient bias voltage of the IC electrode.

Confinement time scalings

Figure 9 (a) shows the confinement time τ of electrons as a function of background neutral gas (hydrogen) pressure P . At the base pressure of 4×10^{-7} Torr and the maximum dipole field coil current of 10.5 kAT, the obtained confinement time is $\tau = 0.5$ s. Assuming that the loss of electrons is caused by the collisions with neutral atoms, the force balance equation of electrons in the confinement phase is given by

$$qn(\mathbf{E} + \mathbf{v}_e \times \mathbf{B}) - m_e n_e v_{en} \mathbf{v}_e = 0.$$

Here the small inertia term is neglected. When the confinement time of electrons is determined by the loss of the momentum of toroidal $\mathbf{E} \times \mathbf{B}$ motion due to the collisions with neutral gas molecules, the toroidal viscous force is balanced by the Lorentz force caused by the outgoing radial velocity of electrons:

$$0 = -en_e v_r B - m_e n_e v_{en} (v_t - v_n),$$

where e is charge, v_r and v_t are radial and toroidal speed of electrons, m_e is electron mass, n_e is electron density, v_n is the velocity of neutral atom, $v_{en} = n_n \sigma v_t$ is the electron-neutral atom mean collision frequency, n_n is neutral gas density, and σ is the collision cross section. Assuming that $v_n = 0$, the radial outgoing velocity of the electrons is given by

$$v_r = \frac{m_e n_n \sigma E^2}{e B^3}.$$

Taking the minor radius of the electron plasma a as the typical length, the typical diffusion time of the electrons is given by

$$\tau_D \sim a/v_r = \frac{eaB^3}{m_e n_n \sigma E^2} \propto P^{-1} B^3.$$

Substituting the experimental parameters of $B \sim 0.005$ T, $P = 10^{-6}$ Torr, $E = 3 \times 10^2$ Vm $^{-1}$, $\sigma \sim 10^{-19}$ m 2 , and $a = 0.1$ m, the typical confinement time τ_D is in the order of 1 s, and it is comparable to the observed confinement time. For the pressure range of 10^{-6} to 10^{-4} Torr, τ is scaled as $\propto P^{-1}$, as shown in Fig. 9 (a), indicating that the effects of residual neutral gas set the confinement time. When P is below $\sim 10^{-6}$ Torr, τ deviates from the P^{-1} line and it saturates near 0.5 s. The confinement time at the base

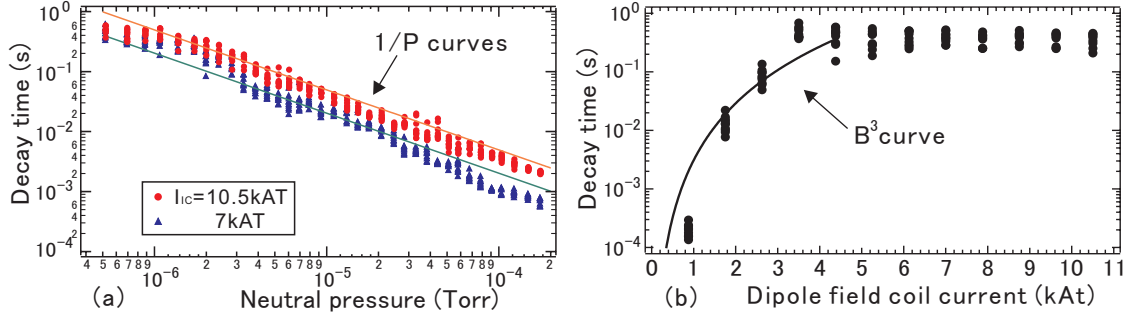


FIGURE 9. Confinement time of toroidal electron plasma in the variation of (a) base pressure and (b) magnetic field strength.

pressure of 4×10^{-7} Torr in the variation of the dipole field coil current is shown in Fig. 9 (b). Before entering the saturation region (when I_{IC} is below ~ 5 kAT), the observed τ is approximately proportional to B^3 and it also agrees with the parameter dependence of the calculated τ_D , but τ has an upper limit in spite of the increase of the magnetic field strength above $I_{IC} \sim 5$ kAT. As indicated in the change of the electron charge in Fig. 9 (b), the amount of the trapped charge as well as τ saturate above $I_{IC} \sim 5$ kAT, although the obtained electron density ($\sim 10^{12} \text{ m}^{-3}$) is far below the Brillouin density limit ($\sim 10^{14} \text{ m}^{-3}$), suggesting the existence of some anomalous loss of the electrons.

In the initial large fluctuation phase just after the stop of the electron injection, charge on the wall decreased from ~ 200 pC to 32 pC, and only small fraction of electrons shows good confinement properties. In comparison with the trapped charge during the electron injection calculated from the Poisson's equation, stably confined electron charge when $I_{IC} = 10.5$ kAT, $P = 4 \times 10^{-7}$ Torr, and $V_{IC} = -300$ V is estimated to be $\sim 5 \times 10^{-8}$ C.

Stabilizing effects of magnetic shear

As described in the previous section, the reduction of electrostatic fluctuation was realized by properly adjusting the potential profiles. The addition of toroidal magnetic field (sheared magnetic field) also can stabilize the diocotron instability. The effects of magnetic shear is also applicable for the stabilization of MHD instability of two-fluid plasmas, and thus it might be potentially effective for the stable confinement of multi-component plasmas.

Electrostatic fluctuations during the electron injection, measured by a wall probe, are shown in Fig. 10 in the variation of added toroidal field. Dipole field coil current $I_{IC} = 7$ kAT was kept constant. When I_{TR} is larger than ~ 4 kAT (the strength of a toroidal field is close to the dipole field strength), the amplitude of the total fluctuation decreases by a factor of 10, compared with when in pure dipole field configuration. During these experiments, the generated space potential is kept approximately constant (ϕ_H of emissive Langmuir probe at $R = 46$ cm is between 230 V and 290 V, for the variation of I_{IC} from 0 kAT to 9 kAT), and stabilization of diocotron instability by

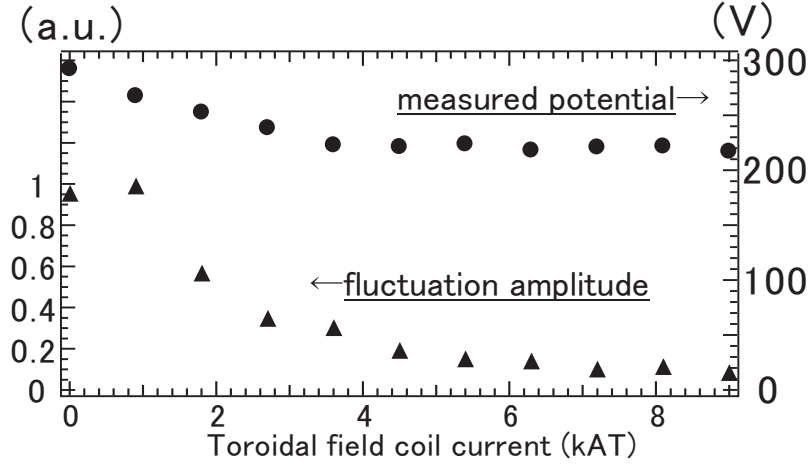


FIGURE 10. Electrostatic fluctuations and space potentials at $R = 46$ cm in the variation of added toroidal field I_{TF} . Fluctuation amplitude is normalized by the absolute value of space potential when $I_{TF} = 0$.

magnetic shear [25] is experimentally demonstrated.

Although the addition of a toroidal magnetic field is effective for the realization of quiet plasma during the electron injection, it induces the earlier onset of the rapid growth of instability after the stop of the electron injection. Figure 11 (a) shows the wall probe signals in the variation of added toroidal field. The stable charge decay, as observed in pure dipole field configuration (Fig. 7), is not realized when the magnetic shear exists. As shown in the life time of the electron plasma as function of toroidal field strength in Fig. 11 (b), the plasma tends to disrupt earlier in the stable confinement phase as the stronger toroidal field is added.

Reduction of the stable confinement time is similarly observed even in the pure dipole field when structures like Langmuir probes are inserted into the confinement region. One of the possible interpretations is that when electrons hit the surfaces of the obstacles, accumulated neutral gas molecules are released and ionized, and it causes the ion resonance instability. When toroidal field is added to the pure dipole field configuration, the $\mathbf{E} \times \mathbf{B}$ drift motions of electrons take spiral orbits around the internal conductor, and the trajectories may intersect the coolant and feeder structures of the internal conductor. Then these effects could lead to the collisions of electrons with the obstacles. In contrast, when electrons are confined in pure poloidal field, the charged particles do not hit the coolant structures as long as they rotate in the toroidal direction due to the $\mathbf{E} \times \mathbf{B}$ drift motion. The addition of toroidal field lead to the increase of space potentials near the bar structure of the IC electrode, indicating that electrons are transported inwardly due to the spiral motion.

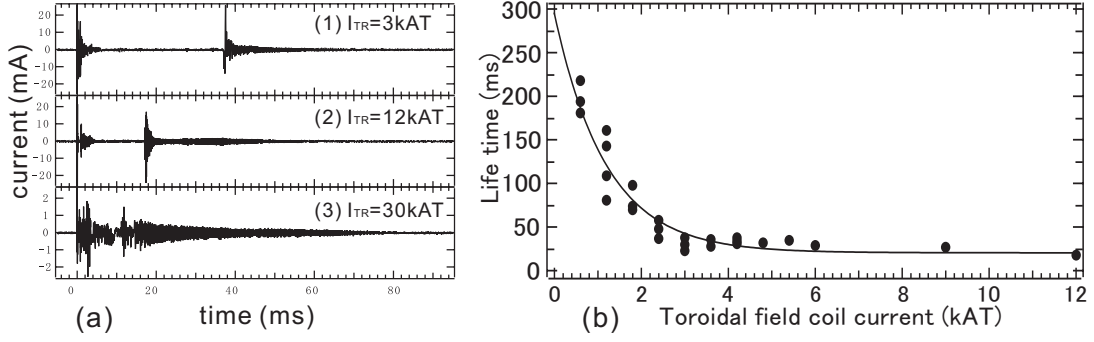


FIGURE 11. (a) Wall probe signals in the variation of added toroidal field. Electrons are injected from $t = -100$ to $0 \mu\text{s}$. (b) Stable confinement time before the rapid growth of the instability.

IV. PROSPECT TOWARD ANTIMATTER PLASMAS AND MULTI-COMPONENT PLASMAS

For the trap of antimatter plasmas and its mixtures, where the particles are supplied from relatively weak radiation sources compared with conventional plasma sources, excellent confinement properties are important for trap devices. The Proto-RT experiments demonstrated the fine confinement properties of non-neutral plasmas in the magnetic surface configuration, and the next task is the injection and simultaneous confinement of another particles to form multi-component plasmas. At present, as well as the experiments of toroidal non-neutral plasmas on internal conductor devices [1], a stellarator [2], and a helical system [24] are in progress or under construction. A helical device can also produce closed magnetic surfaces [2] with only “external” field coils located outside of the plasma.

For the creation of multi-component plasmas, we can inject another species of particles into a magnetic surface configuration by means of several methods. By the combination of dipole and vertical magnetic fields, a magnetic neutral loop is generated between two kinds of coils along the confinement region of plasmas. One can inject charged particles from peripheral region near the magnetic null line [6]. Because the magnetic moment μ is not conserve near X point of the magnetic field lines, the particles take chaotic trajectories with long orbit length. When an electron plasma is generated and stably confined, the electrostatic force caused by the self-space potential can be used for the trap of positrons until the plasma is neutralized. The use of potential well of the initially generated plasma is also effective for other opposite sign of charged particles like positrons and antiprotons. For a device like a helical system, the inductive charging method [11] is an another solution to inject and compress both signs of magnetized charged particles.

V. SUMMARY

As a first step toward the multi-component non-neutral plasmas, experimental investigation into the equilibrium and confinement properties of pure electron plasmas was

carried out in a toroidal magnetic surface configuration. The obtained results are summarized as follows. Long-term stable confinement of a toroidal electron plasma was demonstrated in a magnetic surface configuration. In the initial fluctuating phase, the trapped charge adjusts (diminishes) to enter a quiescent phase, when the potential contours are externally adjusted to the structure of magnetic surfaces. In the present device, we confined electrons with a peak density of an order of 10^{12} m^{-3} and total charge of an order of $\sim 10^{-8} \text{ C}$ for more than 0.1 s. When τ is below $\sim 0.1 \text{ s}$, it is scaled as $\tau \propto P^{-1} B^3$ for the pressure range between 10^{-6} and 10^{-4} Torr, indicating that the collisions with remaining neutral gas limit the confinement of electrons. In the lower pressure region of below $\sim 10^{-6}$ Torr, τ saturates above $\sim 0.1 \text{ s}$, suggesting the anomalous loss of electrons. Although the stabilizing effects of magnetic shear is observed, the addition of toroidal field shortens the stable confinement time, possibly because of the obstacles of the support structure for the internal conductor. The adverse effects of the internal structures are inevitable in the present device, and this problem will be solved in a stellarator [2] or superconducting levitated ring device [1] in future experiments.

ACKNOWLEDGMENTS

The authors would like to acknowledge the useful discussions and advices of Mr. Junji Morikawa, Prof. Haruhiko Himura, and Mr. Hidenori Wakabayashi. This work was funded by a Grant-in-Aid for Scientific Research No. 14102033 from MEXT of Japan. The work of H. S. was supported in part by JSPS Research Fellowships for Young Scientists.

REFERENCES

1. Z. Yoshida et al., Y. Ogawa et al., H. Himura et al., C. Nakashima et al., in *Nonneutral Plasma Physics III*, edited by J. J. Bollinger, R. L. Spencer and R. C. Davidson, AIP Conference Proceedings 498, New York, 1999, pp. 397–422.
2. T. S. Pedersen and A. H. Boozer, *Phys. Rev. Lett.* **88**, 205002 (2002).
3. S. M. Mahajan and Z. Yoshida, *Phys. Rev. Lett.*, **81**, 4863–4866 (1998).
4. Z. Yoshida and S. M. Mahajan, *Phys. Rev. Lett.*, **88**, 095001 (2002).
5. L. C. Steinhauer and A. Ishida, *Phys. Rev. Lett.*, **79**, 3423–3426 (1997).
6. C. Nakashima, Z. Yoshida, H. Himura et al., *Phys. Rev. E*, **65**, 036409 (2002).
7. H. Saitoh, Z. Yoshida, C. Nakashima et al., *Phys. Rev. Lett.*, **92**, 255005 (2004).
8. D. H. E. Dubin and T. M. O’Neil, *Rev. Mod. Phys.*, **71**, 87–172 (1999).
9. M. Amoretti, C. Amsler, G. Bonomi et al., *Nature*, London, 2002, **419**, 456–459.
10. G. Gabrielse, N. S. Bowden, P. Oxley et al., *Phys. Rev. Lett.*, **89**, 213401 (2002).
11. G. S. Janes, *Phys. Rev. Lett.*, **15**, 135–138 (1965).
12. J. D. Daugherty and R. H. Levy, *Phys. Fluids*, **10**, 155–161 (1967).
13. J. D. Daugherty, L. Grodzins, G. S. Janes, and R. H. Levy, *Phys. Rev. Lett.*, **20**, 369–371 (1968).
14. J. D. Daugherty, J. E. Eninger, and G. S. Janes, *Phys. Fluids*, **12**, 2677–2693 (1969).
15. A. Mohri, M. Masuzaki, T. Tsuzuki, and K. Ikuta, *Phys. Rev. Lett.*, **34**, 574–577 (1975).
16. W. Clark, P. Korn, A. Mondelli, and N. Rostoker, *Phys. Rev. Lett.*, **37**, 592–595 (1976).
17. K. Avinash: *Phys. Fluids B*, **3**, 3226–3231 (1991).
18. P. Zaveri, P. I. John, K. Avinash, and P. K. Kaw, *Phys. Rev. Lett.*, **68**, 3295–3298 (1992).
19. S. S. Khirwadkar, P. I. John, K. Avinash et al., *Phys. Rev. Lett.*, **71**, 4334–4337 (1993).
20. M. R. Stoneking, P. W. Fontana, R. L. Sampson, and D. J. Thuecks, *Phys. Plasmas*, **9**, 766–771 (2002).

21. M. R. Stoneking, M. A. Growdon, M. L. Milne, and R. T. Peterson, *Phys. Rev. Lett.*, **92**, 095003 (2004).
22. T. Uchida, *Jpn. J. Appl. Phys.*, **33**, L43–L44 (1994).
23. Z. Yoshida, H. Asakura, H. Kakuno, et al., *Phys. Rev. Lett.*, **81**, 2458–2461 (1998).
24. H. Himura, H. Wakabayashi, M. Fukao et al., *Phys. Plasmas*, **11**, 492–495 (2004).
25. S. Kondoh, T. Tatsuno, and Z. Yoshida, *Phys. Plasmas*, **8**, 2635–2640 (2001).